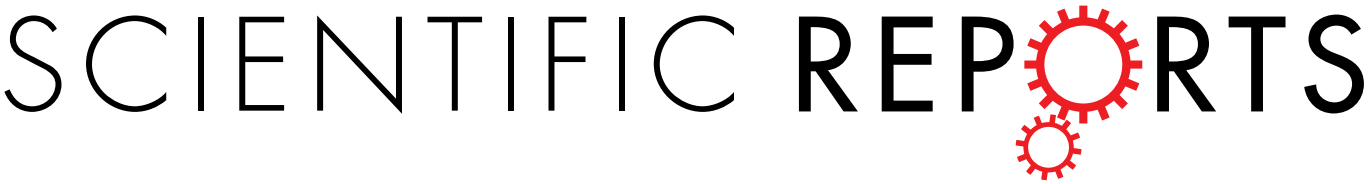

OPEN

$\mathcal{PT}$-symmetric interference transistor

Alexander A. Gorbatsevich[1,2], Gennadiy Ya. Krasnikov[2] & Nikolay M. Shubin[1,2,3]

Received: 26 June 2018
Accepted: 7 October 2018
Published online: 25 October 2018

We present a model of the molecular transistor, operation of which is based on the interplay between two physical mechanisms, peculiar to open quantum systems that act in concert: $\mathcal{PT}$-symmetry breaking corresponding to coalescence of resonances at the exceptional point of the molecule, connected to the leads, and Fano-Feshbach antiresonance. This switching mechanism can be realised in particular in a special class of molecules with degenerate energy levels, e.g. diradicals, which possess mirror symmetry. At zero gate voltage infinitesimally small interaction of the molecule with the leads breaks the $\mathcal{PT}$-symmetry of the system that, however, can be restored by application of the gate voltage preserving the mirror symmetry. $\mathcal{PT}$-symmetry broken state at zero gate voltage with minimal transmission corresponds to the "off" state while the $\mathcal{PT}$-symmetric state at non-zero gate voltage with maximum transmission – to the "on" state. At zero gate voltage energy of the antiresonance coincides with exceptional point. We construct a model of an all-electrical molecular switch based on such transistors acting as a conventional CMOS inverter and show that essentially lower power consumption and switching energy can be achieved, compared to the CMOS analogues.

Implementation of molecules in integrated circuits (IC) offers great advantages due to extreme miniaturization and perfect reproducibility[1–3]. But despite long-term and intensive efforts since its origin in the early 70s[4], molecular electronics (ME) has not yet presented any experimentally realized candidate to replace the silicon transistor as a "wheel-horse" of the modern IC industry. High expectations were held and are still in place with graphene[5] and post graphene organic Dirac materials[6]. During past period ME mainly concentrated on the attempts to reproduce typical elements of silicon electronics[7–12]. In the case of graphene and related materials this approach has been based on the efforts to develop band opening methods[13], which, however, haven't resulted yet in a new IC technology either. On the other hand, due to complex geometry and topology of molecular structures one could expect that the devices with working principles different from the ordinary field-effect and bipolar transistors, could be designed.

The energy spectrum of a molecule manifests itself in transport phenomena by means of resonances. If the molecule possesses different carrier paths, destructive interference can result in formation of asymmetric Fano-Feshbach resonance[14], which combines a resonance (transmission peak) and an antiresonance (transmission dip) nearby. Existence of the interference effect in transport through molecules, which is intensively discussed in the literature[15–19], is now well established experimentally[20–23]. In ref.[24] quantum interference transistor (QIT) was described with the "off" state corresponding to perfect interference destruction of both transmission and current. One of the main challenges in CMOS electronics is reduction of the operating voltage that doesn't follow Moore's law (ITRS 2.0). In ref.[25] it was argued that the interference control of the carrier transport over different paths can substantially reduce the operating gate voltage, because the suppression of the transmission function can be achieved at lower gate voltage compared with the one required to move the transmission function peak away from the distribution function window. However, antiresonances, which arise from the destructive quantum interference (DQI), are determined by the topology of the structure that includes different interfering carrier paths. Hence, variation of the on-site potential and/or intersite hopping can only shift the antiresonance in energy rather than destroy it, because interfering paths are retained under such variations. The voltage required to shift an antiresonance away from the operating energy region is determined by the carrier distribution in the leads on a scale no less than kT and, hence, is not small. Therefore, the proposed control of the transmission resonance by low voltages should rely on a mechanism more complex than multipath interference solely. For a logical gate to operate, its constituting elements (transistors) should undergo transitions between the "off" and the "on"

[1]P.N. Lebedev Physical Institute of the Russian Academy of Sciences, Division of solid state physics, Moscow, 119991, Russia. [2]JSC Molecular Electronics Research Institute, Zelenograd, Moscow, 124460, Russia. [3]Department of quantum physics and nanoelectronics, National Research University of Electronic Technology, Zelenograd, Moscow, 124498, Russia. Correspondence and requests for materials should be addressed to A.A.G. (email: aagor137@mail.ru)

states, with the latter state being even more important than the former one as it provides switching of the successive gate. The "on"/"off" ratio for the transistor conductance should be as high as possible to provide a reliable gate operation. However, this requirement is scarcely achievable in quantum interference transistors operating near the antiresonance because of the low transmission away from the antiresonance[26]. Hence, a quantum transistor is required, which possesses a combination of antiresonance and nearby resonance that is responsible for high conductance in the "on" state.

In this paper we show that, indeed, the transmission probability of a special class of molecules can be controlled in a wide range by applying small gate voltages. This phenomenon can be easily understood with a deep connection between $\mathcal{PT}$-symmetry and scattering problems[27,28]. Coupling of spatially symmetric molecule to electrodes results in $\mathcal{PT}$-symmetry breaking, which is accompanied by coalescence of resonances[29] at the exceptional point of an open quantum system comprised of the molecule and the electrodes[28,30] and transmission decrease. This effect is enhanced by the shift of Fano-Feshbach antiresonance to the EP point. The mentioned special class of molecules consists of systems with degenerate energy levels, e.g. diradicals[31–33] (but not restricted to), which possess mirror symmetry.

Results

Phenomenological model. Consider an open quantum system comprised of a molecule and contacts that possesses EP in a sense of ref.[28]. At this EP two unity resonances coalesce and cancel each other making the transition to the "off" state very sharp. An open quantum system should be spatially symmetric in order to possess EP. To take advantage of both DQI and coalescence of resonances at the EP one should consider a system with two resonances and one antiresonance. The transmission coefficient of an arbitrary two-terminal quantum system can be written in the compact form[28,30]:

$$T(\omega) = \frac{|P(\omega)|^2}{|P(\omega)|^2 + |Q(\omega)|^2}. \tag{1}$$

Here $P(\omega)$ and $Q(\omega)$ are some functions of an energy ω. Real zeroes of function $P(\omega)$ correspond to transmission nodes (antiresonances), while real zeroes of function $Q(\omega)$ determine exact positions of perfect (unity) resonances on the energy axis[28,30]. In the vicinity of the resonances and antiresonance $P(\omega)$ and $Q(\omega)$ can be expressed as[28]:

$$\begin{aligned} P(\omega) &= 2\Gamma B(\omega - \varepsilon_0)D_P, \\ Q(\omega) &= (\omega - \varepsilon_1^{+})(\omega - \varepsilon_1^{-})D_Q, \end{aligned} \tag{2}$$

where ε_0 and $\varepsilon_1^{\pm}$ determine exact position of the transmission antiresonance and resonances, correspondingly, Γ is the imaginary part of the contact self-energy describing interaction of a molecule with the leads[34,35] and B is some positive dimensionless coefficient. Factors D_P and D_Q take into account the contributions from the remote energy levels and can be estimated as $D_P \sim D_Q \sim \Delta^{N-2}$, where Δ is an average distance between the remote energy levels and N is the dimension of the molecular orbital Hilbert space. Phenomenologically, functions $P(\omega)$ and $Q(\omega)$ are defined up to an arbitrary common factor, hence, we can redefine the parameter $B \mapsto BD_P/D_Q$ and replace three phenomenological parameters B, D_P and D_Q by just B. Further we will use B as such generalized parameter.

Consider a model that possesses degenerate antiresonance and resonance levels in the symmetric phase, which can be distorted by an external perturbation described by parameter δ. Energies of the antiresonance ε_0 and resonances $\varepsilon_1^{\pm}$ can be expressed as:

$$\begin{aligned} \varepsilon_0 &= x_0\delta, \\ \varepsilon_1^{\pm} &= x_1\delta \pm \sqrt{y^2\delta^2 - z^2\Gamma^2}. \end{aligned} \tag{3}$$

Here $x_{0,1}$, y and z are some dimensionless parameters depending on the structure of a particular system. Terms in Eq. (3), which are linear in δ, describe the shift of the (anti)resonance positions due to the external perturbation and non-analytical term (square root) in the expression for $\varepsilon_1^{\pm}$ describes the coalescence of resonances phenomenon. Energy of the degenerate state (at $\delta = 0$) is set to the energy origin. One should bare in mind that degenerate levels occur only in multiply-connected structures (in simple-connected, e.g. linear, all energy levels are non-degenerate). In such systems antiresonances naturally appear as well ($P(\omega) = 0$). If the external perturbation δ is high enough ($\delta > \delta_{EP} = zy^{-1}\Gamma$), then the transmission has two unity peaks at $\omega = \varepsilon_1^{\pm}$, which coalesce at $\delta = \delta_{EP}$. This is the EP, which is associated with $\mathcal{PT}$-symmetry breaking. For small δ or, equivalently, for strong enough coupling with the leads ($\delta < \delta_{EP}$) the roots of $Q(\omega)$ in (2) are complex. Therefore $|Q(\omega)|$ is non-zero for any real energy ω and the transparency is always less than unity. The poorest transmission profile (i.e. the "off" state) corresponds to $\delta = 0$. From Eqs (1–3) one can see, that in this case there are two peaks at $\omega = \pm z\Gamma$ with

$$T_{peak}(\omega = \pm z\Gamma;\ \delta = 0) = \frac{B^2}{B^2 + z^2}, \tag{4}$$

separated by a zero dip at $\omega = 0$.

Microscopic model. The above described phenomenological properties of the transmission coefficient can be realized within the following microscopic model. There are two degenerate states $|1\rangle$ and $|2\rangle$ with the same energy ε. This system is attached symmetrically to two leads (left and right) in such a way that the mirror symmetry operation σ_{LR}, which maps the left lead into the right one and vice versa, is also an element of the symmetry

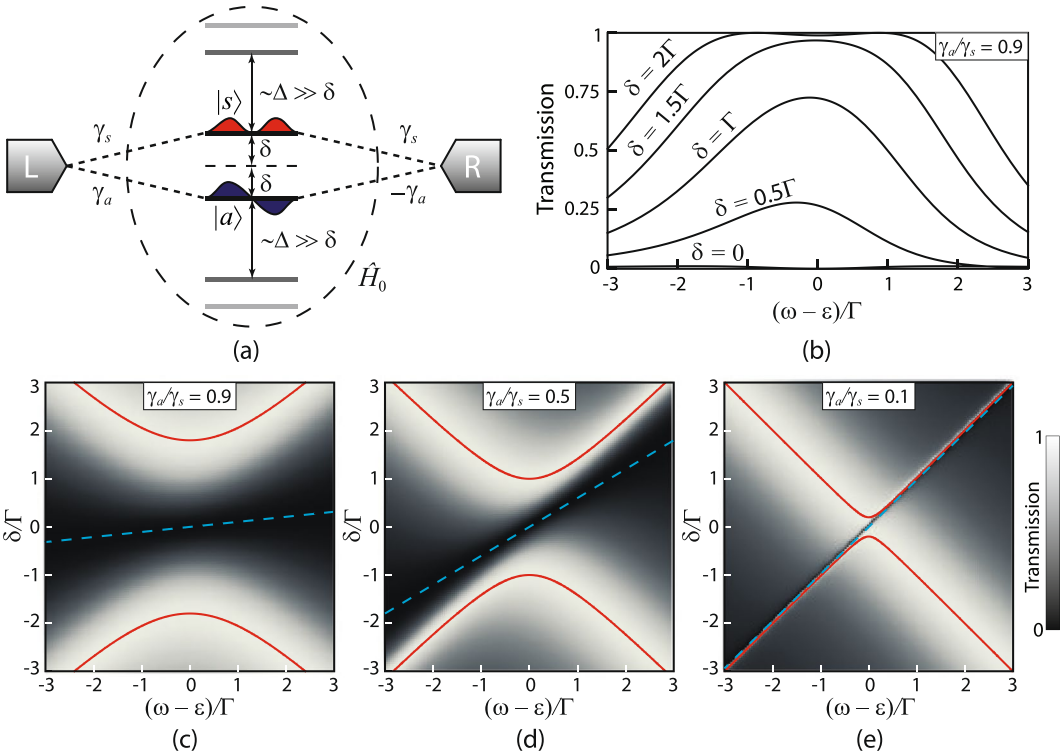

Figure 1. Microscopic model and its transmission coefficient. (**a**) Schematic view of the microscopic model of the molecular system depicting symmetric $|s\rangle$ and anti-symmetric $|a\rangle$ states connected to the leads by couplings (5). Γ is set as energy unit and $k_a = -k_s = 1$ for convenience. Evolution of the transmission coefficient profile with variation of δ (γ_s is set to 1 and $k_a = -k_s = 1$) for (**b**) some discrete values of δ for $\gamma_a = 0.9$, and (**c**–**e**) in the form of density plots for (**c**) $\gamma_a = 1$, (**d**) $\gamma_a = 0.5$ and (**e**) $\gamma_a = 0.1$. Red solid lines indicate the position of perfect resonances and dashed cyan–zeros of the transmission.

group G of the bare Hamiltonian of the system, i.e. $\sigma_{LR} \in G$. Due to the degeneracy, there must be an irreducible representation of the symmetry group G acting on the subspace $\mathcal{H}_{12} = Span(|1\rangle, |2\rangle)$ of the total Hilbert space of states of the isolated system. Let us choose the basis in $\mathcal{H}_{12}$ as the basis of a symmetric $|s\rangle$ and an anti-symmetric $|a\rangle$ states, which are the eigenstates of the reflection operator σ_{LR}: $\sigma_{LR}|s\rangle = |s\rangle$ and $\sigma_{LR}|a\rangle = -|a\rangle$. These states conserve their symmetry with introduction of the perturbation, which is invariant under σ_{LR}. The tunnelling matrix elements between the leads and the symmetric state are of the same sign, whereas, the tunnelling matrix elements between the leads and the anti-symmetric state are of opposite signs (see Fig. 1a). Therefore in this basis couplings to the leads can be written as

$$\begin{aligned} \mathbf{u}_L &= \sqrt{\Gamma}\begin{pmatrix}\gamma_s\\ \gamma_a\end{pmatrix}, \\ \mathbf{u}_R &= \sqrt{\Gamma}\begin{pmatrix}\gamma_s\\ -\gamma_a\end{pmatrix}. \end{aligned} \tag{5}$$

Here Γ governs the coupling strength and positive dimensionless parameters $0 \le \gamma_{s,a} \le 1$ describe relative couplings of symmetric and anti-symmetric states to the leads. Parameters $\gamma_{s,a}$ can be calculated, for example, as projections of the vector $\Gamma^{-1/2}\mathbf{u}^{site}_{L,R}$ onto $|s\rangle$ or $|a\rangle$ respectively, where $\mathbf{u}^{site}_{L,R}$ describes the coupling to the leads in the site (atomic orbitals) basis. If each lead is attached to only one site, then $\gamma_{s,a}$ is just a contribution of the state localized in the connection site to the symmetric or anti-symmetric state correspondingly (see Supplementary Materials).

Application of the gate voltage introduces external perturbation that lowers the symmetry of the system, resulting in removal of the degeneracy. Suppose that the external perturbation lowers the symmetry of the system from the group G to its some non-trivial subgroup $H \subset G$, such that $\sigma_{LR} \in H$. This perturbation introduces detuning of the energy of symmetric and anti-symmetric states: $\varepsilon_{s,a}(\delta) = \varepsilon + k_{s,a}\delta$ with $\delta > 0$ and dimensionless parameters $-1 \le k_{s,a} \le 1$ accounting for the different influence of the perturbation on the energies of symmetric and anti-symmetric states (see Fig. 1a). Parameters $k_{s,a}$ can be estimated, for instance, from the perturbation theory (see Supplementary Materials for details); note that $k_a \ne k_s$ as the considered perturbation removes the degeneracy. Assume that couplings (5) are not affected by this perturbation. In fact, Γ and $\gamma_{s,a}$ are some smooth functions of the perturbation strength, i.e. δ. However, taking this into account does not change the qualitative picture described below. The transport through the states $|s\rangle$ and $|a\rangle$ (neglecting the contribution from remote states to the transport process) within the wide-band limit[35] can be described by the transmission coefficient in the form (1) with the following P and Q functions (see Methods section):

$$\begin{aligned} P(\omega) &= 2\det(\omega\hat{I} - \hat{H}_0) \times \mathbf{u}_L^{\dagger}(\omega\hat{I} - \hat{H}_0)^{-1}\mathbf{u}_R, \\ Q(\omega) &= \det(\omega\hat{I} - \hat{H}_{aux}). \end{aligned} \tag{6}$$

Here

$$\hat{H}_0 = \begin{pmatrix} \varepsilon + k_s\delta & 0 \\ 0 & \varepsilon + k_a\delta \end{pmatrix} \tag{7}$$

is the bare Hamiltonian of the system (without taking the leads into account),

$$\hat{H}_{aux} = \hat{H}_0 + i\mathbf{u}_L\mathbf{u}_L^{\dagger} - i\mathbf{u}_R\mathbf{u}_R^{\dagger} = \begin{pmatrix} \varepsilon + k_s\delta & 2i\Gamma\gamma_s\gamma_a \\ 2i\Gamma\gamma_s\gamma_a & \varepsilon + k_a\delta \end{pmatrix} \tag{8}$$

is the non-Hermitian auxiliary Hamiltonian with its real eigenvalues corresponding to energies of perfect transmission[28], and $\hat{I}$ is the 2×2 identity matrix. Hamiltonian $\hat{H}_{aux}$ is $\mathcal{PT}$-symmetric, where $\mathcal{P} = \sigma_{LR}$ denotes to the mirror reflection and $\mathcal{T}$ is the time reversal operator (complex conjugation). Indeed, one can easily check that operator $\mathcal{PT}\hat{H}_{aux}\mathcal{PT}$ acts on any vector $\mathbf{v} \in \mathbb{C}^2$ in the same way as operator $\hat{H}_{aux}$. Thus, $\hat{H}_{aux}$ is $\mathcal{PT}$-symmetric[36]. Therefore, it can possess real eigenvalues, which correspond to perfect transmission peaks, and for certain parameters they can coalesce and the $\mathcal{PT}$-symmetry of the Hamiltonian $\hat{H}_{aux}$ will be broken, leading to coalescence of perfect resonances into one peak with amplitude lower than 1. Moreover, such resonance coalescence is accompanied by symmetry breaking of electron occupation at the energy corresponding to the transmission peak (see Methods for details).

Using Eqs (5–8), the transmission coefficient can be written as:

$$T(\omega) = \frac{4\Gamma^2[(k_a\gamma_s^2 - k_s\gamma_a^2)\delta - (\gamma_s^2 - \gamma_a^2)(\omega - \varepsilon)]^2}{4\Gamma^2[(k_a\gamma_s^2 - k_s\gamma_a^2)\delta - (\gamma_s^2 - \gamma_a^2)(\omega - \varepsilon)]^2 + \left\{\left[\omega - \varepsilon - \frac{1}{2}\delta(k_a + k_s)\right]^2 + 4\gamma_s^2\gamma_a^2\Gamma^2 - \delta^2\frac{(k_a - k_s)^2}{4}\right\}^2}. \tag{9}$$

From this formula one can see that for a sufficiently large detuning δ there are two unity peaks of transmission (zeros of Q, i.e. eigenvalues of $\hat{H}_{aux}$) at $\omega = \varepsilon + \frac{1}{2}\delta(k_a + k_s) \pm \sqrt{\frac{1}{4}\delta^2(k_a - k_s)^2 - 4\gamma_s^2\gamma_a^2\Gamma^2}$. Decreasing the detuning one can achieve the coalescence of resonances at $\delta = 4\gamma_s\gamma_a\Gamma|k_a - k_s|^{-1}$, which corresponds to the EP of $\hat{H}_{aux}$. Further decreasing δ results in further lowering of the transmission coefficient peak. There is also a zero-valued antiresonance (zero of P) at $\omega = \varepsilon + \delta(k_a\gamma_s^2 - k_s\gamma_a^2)/(\gamma_s^2 - \gamma_a^2)$, which additionally lowers the transmission with decreasing δ. One can see that, moving the energy origin to ε, Eq. (9) takes the phenomenological form described by Eqs (1–3) with the following phenomenological parameters:

$$B = |\gamma_s^2 - \gamma_a^2| \quad x_0 = \frac{k_a\gamma_s^2 - k_s\gamma_a^2}{\gamma_s^2 - \gamma_a^2}, \quad x_1 = \frac{k_a + k_s}{2}, \quad y = \frac{|k_a - k_s|}{2}, \quad z = 2\gamma_s\gamma_a. \tag{10}$$

Thus, according to Eq. (4) one can see that the poorest transmission peaks (at $\delta = 0$) are

$$T_{peak}(\omega = \varepsilon \pm 2\gamma_s\gamma_a\Gamma;\ \delta = 0) = \frac{(\gamma_s^2 - \gamma_a^2)^2}{(\gamma_s^2 + \gamma_a^2)^2}. \tag{11}$$

From (10) we see that there is a limiting case $\gamma_s/\gamma_a \to 1$ that results in $B \to 0$ and $x_0 \to \infty$, while the product $Bx_0 \to \gamma_{s,a}^2(k_a - k_s)$ remains finite. In this case complete opaqueness, i.e. $T \equiv 0$, can be obtained for $\delta = 0$. In practice, however, the transmission never vanishes because of the transport through remote energy levels, which are not taken into account in this model. Evolution of the transmission coefficient profile (9) with variation of δ for different ratios of the parameters γ_s and γ_a is illustrated in Fig. 1c–e. It is important to note that for a single-level system (i.e. $\gamma_a = 0$ or $\gamma_s = 0$), where the $\mathcal{PT}$-symmetry breaking is absent, T_{peak} equals unity identically.

Quantum interference inverters based on $\mathcal{PT}$-symmetric interference transistors. Consider a quantum analogue of CMOS inverter consisting of two quantum switches, connected between one common output lead and two reference voltage sources with voltages V_{ref1} and V_{ref2}, respectively. Input signal V_{in} is applied to the common gate of these switches, which is galvanically isolated from the system. Figure 2 depicts two examples of such quantum interference inverters. For a high-resistance load we can implicitly evaluate the voltage transfer characteristic $V_{out}(V_{in})$ of this inverter and estimate its maximum negative gain, which is achieved at $V_{in} = \frac{1}{2}(V_{ref1} + V_{ref2})$ due to the symmetry (see Methods):

$$\begin{aligned} G_{max} &= G\left(V_{in} = \frac{V_{ref1} + V_{ref2}}{2}\right) \\ &= \sinh\frac{e\Delta V}{2kT} \times \frac{256\alpha^2\Gamma^2\gamma_a^2\gamma_s^2(k_a - k_s)^2kTe\Delta V}{\left[16\Gamma^2\left(\gamma_s^2 - \gamma_a^2\right)^2 + \alpha^2(k_a - k_s)^2e^2\Delta V^2\right]\left[16\Gamma^2\left(\gamma_s^2 + \gamma_a^2\right)^2 + \alpha^2(k_a - k_s)^2e^2\Delta V^2\right]}. \end{aligned} \tag{12}$$

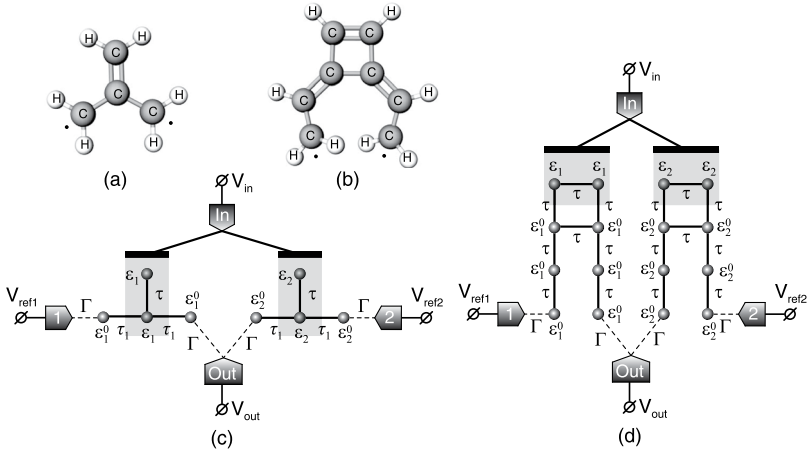

Figure 2. Diradical based quantum inverters. Structural model of diradical configuration of (**a**) trimethylenemethane molecule (non-disjoint) and (**b**) divinylcyclobutadiene molecule (disjoint). Schemes of quantum interference inverters, composed of two quantum switches based on (**c**) non-disjoint diradicals and (**d**) disjoint diradicals. Molecules are shown in the form of their Hückel theory tight-binding graphs corresponding to their carbon skeleton. Shaded regions indicate the atoms, which are electrostatically affected by the input gate.

Here $\Delta V = V_{ref2} - V_{ref1}$ is fixed by the external supply voltage. In the saturation regime ($e\Delta V \gg kT$) the maximum value of G grows exponentially with ΔV due to the factor $\sinh\frac{e\Delta V}{2kT}$. For $e\Delta V \lesssim kT$ (in the ohmic regime) it becomes independent of the temperature and we can estimate the minimum difference of the reference voltages (supply voltage) ΔV_{crit} needed to make the inverter operate, i.e. which provides $G_{max} = 1$:

$$\Delta V_{crit} \approx \frac{4\Gamma}{e\alpha|k_a - k_s|}\sqrt{4\gamma_a^2\gamma_s^2 - \gamma_a^4 - \gamma_s^4 - 2\gamma_a\gamma_s\sqrt{5\gamma_a^2\gamma_s^2 - 2\gamma_a^4 - 2\gamma_s^4}} \sim |\gamma_s - \gamma_a| \text{ as } \frac{\gamma_a}{\gamma_s} \to 1. \tag{13}$$

From Eq. (13) one can see that ΔV_{crit} can become infinitesimal as $\gamma_a/\gamma_s \to 1$. On the other hand, however, G_{max} remains bounded in the ohmic regime even if $\gamma_a/\gamma_s \to 1$. From the analysis of Eq. (12) one can conclude that for $\Delta V = 4\frac{\Gamma}{e\alpha\,|\,k_a - k_s|}\sqrt{|\gamma_s^4 - \gamma_a^4|}$ the gain G_{max} reaches its maximum: $2(\gamma_s/\gamma_a)^2$ for $\gamma_s < \gamma_a$ or $2(\gamma_a/\gamma_s)^2$ for $\gamma_s > \gamma_a$. Hence, the steepest negative gain of the voltage transfer characteristic is limited to -2. Nevertheless, it is suitable for operation of the inverter.

Model examples of real molecular structures. Possible candidates for a physical realization of the proposed quantum switch are molecules with degenerate states, e.g. diradicals[31], which are already known for providing transmission antiresonances[32]. Moreover, linkers can stabilize diradical character of such molecules[37]. Hence, we can expect that connection of certain contacts to them will not destroy the degeneracy of the states, but rather stabilize it. Diradicals can be classified into two types: disjoint and non-disjoint depending on how their non-bonding orbitals intersect (i.e. whether they have common atomic orbitals or not). It was shown that simple starring procedure can distinguish between these two types[38,39]. Disjoint diradicals seem to be the most appropriate candidate for our quantum switch. Indeed, applying contacts to atoms comprising different degenerate orbitals means that symmetric and antisymmetric combinations of these orbitals will be connected to the leads by equivalent coupling strength, i.e. parameters γ_s and γ_a [introduced in Eq. (5)] in this case can be made equal (at least within the nearest neighbour tight-binding approximation). As was highlighted above, according to Eq. (11) this leads to zero conductance in the "off" state.

Operation principle of quantum interference inverter requires that one switch must be in the "on" state and another in the "off" state. There are two possible ways of dealing with this task. First of all, one can choose two different quantum systems (molecules) to make two quantum switches that is similar to the conventional CMOS, where there are two different types of transistors: n-channel MOS and p-channel MOS. This approach requires a technology of synthesis of two different molecules with strictly given parameters. On the other hand, we can use the same quantum system (molecule) to create both switches, but influence their spectrum in different ways by additional gates. This method needs only one type of molecule to be synthesised, but the introduction of additional gates results in some complication of the conventional technological process. In the following subsections we consider some schematic examples of quantum inverters with the same molecules in both switches. Different energies of the on-site atomic states are assumed to be achieved by a certain configuration of additional gates (e.g. backgates).

Model of non-disjoint diradical. The first example structure we consider is a model of the trimethylenemethane molecule, which is a non-disjoint diradical[32]. Schematically the quantum inverter structure composed of two such four-atomic (carbon skeleton) molecules is shown in Fig. 2a. Presented schematic model corresponds to a tight-binding Hückel structure of one of the resonance configurations of the trimethylenemethane, which is

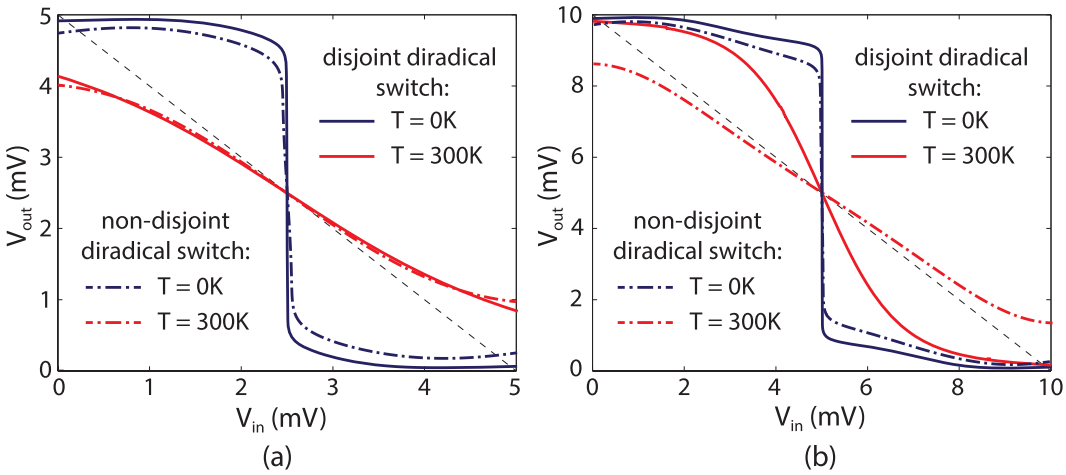

Figure 3. Numerically calculated voltage transfer characteristics for the quantum inverter based on $\mathcal{PT}$ -symmetric interference transistors for room and zero temperature. Supply voltage is $V_0 = 5$ mV (**a**) and $V_0 = 10$ mV (**b**). The inverter operates at zero temperature better than at room temperature. Dashed black line shows the -1 slope for comparison.

stabilized as it coincides in symmetry with the leads couplings. Hence, hopping integral τ is assumed to be greater than τ_1 as it corresponds to a higher bond order. The transmission coefficient, phenomenological, and microscopical parameters of such switches are presented in the Supplementary Material.

We apply the reference voltages as follows: $V_{ref1} = 0$ and $V_{ref2} = V_0$ is the supply voltage. The range of the input voltage, thus, is $0 \leq V_{in} \leq V_0$. Applied input potential changes only some on-site energies of the system (in the shaded region in Fig. 2a). We take this into account in the following form:

$$\varepsilon_{1,2} = \varepsilon_{1,2}^0 + \alpha(eV_{in} - \varepsilon_{1,2}^0). \tag{14}$$

The electrostatic influence of the reference and output leads can also be taken into account in a way similar to (14). It can be shown that this influence only distorts the voltage transfer characteristic and taking it into account is not obligatory to illustrate the operation principles of the quantum interference inverters.

Consider the following example: $\varepsilon_1^0 = eV_{ref1} = 0$, $\varepsilon_2^0 = eV_{ref2} = eV_0$, $\alpha = 0.5$, $\tau_1 = 2.75$ eV, $\tau = 3.65$ eV and $\Gamma = 1$ meV. Energies are measured from the Fermi level of the first reference lead. Here we take typical values of the hopping integrals for single and double bonds (τ_1 and τ correspondingly)[40]. Figure 3a shows voltage transfer characteristics of the inverter for $V_0 = 5$ mV and Fig. 3b for $V_0 = 10$ mV (by dot-dashed lines in both cases). In the latter case the voltage transfer characteristic is obviously better because of higher negative gain achieved.

Model of disjoint diradical. Another example we consider is a model of the divinylcyclobutadiene molecule, which is a disjoint diradical[32]. Schematically the quantum inverter structure composed of two such molecules is shown in Fig. 2b. Presented model corresponds to a simple tight-binding Hückel structure of the divinylcyclobutadiene molecule with all bonds treated as equal, providing equal tunnelling matrix elements τ between p-orbitals of carbon atoms. The transmission coefficient, phenomenological, and microscopical parameters of such switches are presented in the Supplementary Material.

We assume that the applied input voltage changes only on-site energies in the shaded region in Fig. 2b, which is taken into account similarly to Eq. (14). Figure 3a shows voltage transfer characteristics of this inverter for $V_0 = 5$ mV and Fig. 3b for $V_0 = 10$ mV (by solid lines in both cases) for the following parameters: $\varepsilon_1^0 = eV_{ref1} = 0$, $\varepsilon_2^0 = eV_{ref2} = eV_0$, $\alpha = 0.5$, $\Gamma = 1$ meV, and typical value of the hopping integral $\tau = 3$ eV for conjugated hydrocarbons[40].

For higher supply voltage transfer characteristic of the inverter based on the disjoint diradical switches (solid lines in Fig. 3b) show higher maximum absolute value of the gain rather than for the inverter based on the non-disjoint diradical switches (dot-dashed lines in Fig. 3b). This is expectable as disjoint diradicals provide $\gamma_s/\gamma_a = 1$ and, thus, the "off"-state current of such switch becomes smaller (it differs from zero only due to the presence of the "background" transmission arising from remote resonance peaks). However, for smaller supply voltage (Fig. 3a), this "background" component may become high enough to cancel out the key benefit of the disjoint diradical ($\gamma_s/\gamma_a = 1$). Moreover, for disjoint diradicals the degeneracy is removed only in the second order of perturbation (i.e. $k_{a,s}$ become functions of δ). Hence, for lower supply voltages, the sensitivity to the gate voltage decreases compared to non-disjoint diradicals. In this case the transfer characteristic of a non-disjoint diradical based quantum inverter turns out to have slightly more gain (Fig. 3a). From Fig. 3 we see that for our particular parameters chosen only divinylcyclobutadiene can provide a working inverter at room temperature with 10 mV supply voltage.

Discussion

We have shown that there is a fundamental difference between resonant tunnelling through a non-degenerate and a doubly degenerate state. It arises from the effect of an antiresonance formation (because of destructive interference of electron flows through both degenerate states) and the coalescence of resonances, which can be well described by the concept of the $\mathcal{PT}$-symmetry breaking[28]. Thus, one can utilize this phenomenon and use the degenerate quantum system spectrum to construct the quantum interference switch. In comparison with numerous other proposals of molecular interference transistors we should emphasize that our solution has important advantages: it is an all-electrical device (i.e. electric current is controlled by an applied voltage), it can possess extremely low operating voltage (even at room temperature) and our $\mathcal{PT}$-symmetry based model provides a straightforward design rules for constructing such a transistor, which we demonstrated by the examples of specific disjoint and non-disjoint diradicals. Thus, this might be a way to dramatically lower the supply voltage, which now cannot be made lower than 0.5–1 V[41] for the conventional silicon electronic devices, even for promising tunnel field-effect transistors (FET)[42]. Advanced technology of FETs with carbon nanotube (CNT) channel[43] also provides a variety of advantages over the bulk Si electronics[10,44], but sufficient reduction of the supply voltage is not among them. A separate approach is based on a development of non-electronic logical gates, based on, e.g., exciton[45,46] or even heat flow[47] control. Typically such devices has input and output signal of different nature and are designed for optoelectronic[45] or optomechanical[46] applications, rather than for large-scale integration.

Performance of real devices is limited by noise. It is especially significant for low supply voltages. Noise in quantum systems is not distinguished into thermal and shot, it is always a superposition of both and it can be described by a closed expression[48]. Nevertheless, it is illustrative to discuss these contributions independently. Shot noise spectral power is proportional to the current through the system and, thus, it becomes negligible as the voltages and, correspondingly, the currents are scaled down. On the other hand, at finite (room) temperature thermal noise can influence the transport dramatically. Thus, thermal noise is one of the limiting factors of lowering the supply voltage[41].

The mean-square voltage uncertainty is $\Delta V_{therm} = \sqrt{kT/C}$, where C is the capacitance of the load, which is typically the gate capacitance of the next switch. Therefore, using several molecules in parallel in the single switch and, consequently, a bigger gate contact, will increase the capacitance C and lower the noise. But, on the other hand, the greater C is, the worse switching rate $\nu \sim (\tau)^{-1} = (RC)^{-1}$ can be achieved. Here the resistance R can be estimated from the current in the "on" state (see Supplementary Material): $R \approx \frac{h}{e^2} \times \frac{2kT}{\pi\Gamma}$. Assuming the gate is about 10×10 nm lying on 2 nm thick dielectric with $k \approx 5$, we can estimate its capacitance to be about 2aF. This means that without noise taken into account we can expect switching frequencies to be of order of 500 GHz even for low conducting "on" state with $R \approx 1\,\mathrm{M}\Omega$ ($\Gamma \approx 0.04\,kT$ for room temperature). However, noise dramatically lowers the possible operating frequency. Indeed, restricting the minimum operating frequency ν_{min}, one can estimate the minimum allowed supply voltage, which we take to be 8 times the noise voltage uncertainty to provide an error probability at about 10^{-15}[41]. Finally we arrive at the following restriction:

$$V_0 > \sqrt{2\frac{h}{e^2} \times \frac{2(kT)^2}{\pi\Gamma} \times \nu_{min}}, \tag{15}$$

which for the room temperature and $\Gamma \approx 1$ meV gives $V_0 \gtrsim 10\ \mathrm{mV} \times \sqrt{\nu_{min}}$, where ν_{min} is in GHz. Thus, sub-kT/e supply voltages seems to be possible up to $\nu \approx 7$ GHz. More detailed analysis of noise impact on operation of quantum interference gates will be presented elsewhere, as well as consideration of technological parameter variation resulting in asymmetry of the inverter structure.

Our model is based on Hückel theory and does not account for electron repulsion. In ref.[17] it has been shown that DQI predicted by Hückel model does survive in alternant hydrocarbons even with Coulomb effects being taken into account. Diradicals, which we consider, are alternant, hence, we expect that DQI will persist in a more realistic model either. On the other hand, a role of electron repulsion (Coulomb blockade), which is detrimental in the case of weak coupling of a molecule with contacts, is less significant in the case of strong coupling. We have performed tight-binding simulations with increased value of electrode-molecule coupling $\Gamma = 0.1$ eV and $\Gamma = 0.2$ eV (see Supplementary). We have shown that such a value of Γ still retains switching properties of interference transistor but makes operating voltage larger. Thus, the supply voltage cannot be made arbitrary low, as can be provided by an idealized model, but its lower bound should be determined from the optimal value for Γ, which, on the one hand, prevents the Coulomb blockade and, on the other hand, provides sharp enough transmission peaks resulting in sufficient contrast of the switching current. By no means the study of the interplay of electrode-molecule coupling strength and electron repulsion in DQI sensitive molecular transport based on *ab initio* simulations will be of great interest. In our model DQI acts in concert with $\mathcal{PT}$-symmetry breaking at the exceptional point, which is accompanied by coalescence of resonances and sharp decrease of electron transmission. $\mathcal{PT}$-symmetry breaking in quantum conductor possesses a close resemblance with equilibrium phase transitions in condensed matter[28,30]. Hence, we expect that the model proposed in our manuscript should retain efficiency with Coulomb interactions included due to the fact that it is related to the symmetry properties of the system. But the general impact of Coulomb interactions on the behaviour of a quantum conductor near the $\mathcal{PT}$-symmetry breaking transition at the exceptional point is quite a new interesting problem, which deserves special study.

It is also important to admit that we consider an idealized model of the quantum transport process within this paper. Nevertheless, a few steps toward a realistic description can be made, e.g. (see Supplementary): going beyond the wide-band approximation and taking into account electrostatic influence of the reference voltage sources. It turns out that qualitatively our results are valid in more realistic situations as well. However, in order to verify them, one should provide a full numerical calculation for the electronic structure of the considered system, which we plan to perform in our further publications.

At the moment practical realization of high scale integration of quantum molecular gates is beyond the reach of modern technology. However continuous progress in self-assembling methods and, especially, development of atomic precision lithography could make almost inevitable the implementation of molecular gates as building blocks of ICs. We hope that the idea of using degenerate energy levels (e.g. diradicals, but not obligatory) to create molecular switches could open a new field of research.

Methods

Microscopic model: auxiliary Hamiltonian and its exceptional point. Conductance of a quantum conductor is defined by its tunnelling transmission coefficient[49], which can be calculated by the standard formula[50] derived from the nonequilibrium Green's function formalism[34,51,52]:

$$T = 4Tr(\hat{\Gamma}_R \hat{G}^r \hat{\Gamma}_L \hat{G}^a), \tag{16}$$

where $\hat{G}^{r,a}$ is the retarded/advanced Green function and $\hat{\Gamma}_{L,R} = \mathbf{u}_{L,R}\mathbf{u}_{L,R}^{\dagger}$[53] is the coupling matrix (imaginary part of corresponding contact self-energy) to the left or to the right lead. Here $\mathbf{u}_{L,R}$ are vectors, describing couplings of the states of the isolated system to the left/right lead. The traditional approach within the wide-band limit (neglecting real parts of the contact self-energy) leads to the following expression for the transmission[28]:

$$T = \frac{4\left|\det(\omega\hat{I} - \hat{H}_0)\right|^2 \left|\mathbf{u}_R^{\dagger}(\omega\hat{I} - \hat{H}_0)^{-1}\mathbf{u}_L\right|^2}{\left|det(\omega\hat{I} - \hat{H}_{eff})\right|^2}, \tag{17}$$

where $\hat{H}_{eff} = \hat{H}_0 - i\mathbf{u}_L\mathbf{u}_L^{\dagger} - \mathbf{u}_R\mathbf{u}_R^{\dagger}$ is the Feshbach effective Hamiltonian. Following general formalism form ref.[28], one can show that transmission (17) can be written in the form (1). For our microscopic model this can be easily checked using Eqs (5) and (7). Indeed, the following identity holds true:

$$\begin{aligned} |Q|^2 &= \left|\det(\omega\hat{I} - \hat{H}_0 - i\mathbf{u}_L\mathbf{u}_L^{\dagger} + i\mathbf{u}_R\mathbf{u}_R^{\dagger})\right|^2 = \left|\det(\omega\hat{I} - \hat{H}_0 + i\mathbf{u}_L\mathbf{u}_L^{\dagger} + i\mathbf{u}_R\mathbf{u}_R^{\dagger})\right|^2 \\ -4\left|\det(\omega\hat{I} - \hat{H}_0)\right|^2 &\left|\mathbf{u}_R^{\dagger}(\omega\hat{I} - \hat{H}_0)^{-1}\mathbf{u}_L\right|^2 = [4\Gamma^2\gamma_a^2\gamma_s^2 + (\omega - \varepsilon - k_s\delta)(\omega - \varepsilon - k_a\delta)]^2. \end{aligned} \tag{18}$$

Hence, from Eq. (18) we see that within the wide-band limit, the transmission of our system can be written in the form (1) with $P = 2\det(\omega\hat{I} - \hat{H}_0)\mathbf{u}_R^{\dagger}(\omega\hat{I} - \hat{H}_0)^{-1}\mathbf{u}_L$ and $Q = \det(\omega\hat{I} - \hat{H}_{aux})$, where $\hat{H}_{aux}$ is from Eq. (8).

Real eigenvalues of the auxiliary Hamiltonian define the exact location of perfect transmission resonance and, being $\mathcal{PT}$-symmetric it can experience $\mathcal{PT}$-symmetry breaking, which results in resonance coalescence. This is accompanied by the symmetry breaking of electron occupation in the transmission maximum. The matrix of occupations per unit energy $\hat{n}$ can be calculated within NEGF formalism[34]:

$$\hat{n} = \frac{1}{2\pi}[f_L(\omega)\hat{G}^r\hat{\Gamma}_L\hat{G}^a + f_R(\omega)\hat{G}^r\hat{\Gamma}_R\hat{G}^a], \tag{19}$$

where $f_{L,R}$ is the Fermi-Dirac distribution function in the left/right lead. Now suppose that symmetric and anti-symmetric states in the site basis are $|s\rangle = (s_1, s_2, ..., s_N)^{\mathrm{T}}$ and $|a\rangle = (a_1, a_2, ..., a_N)^{\mathrm{T}}$. Thus, neglecting the contribution from distant energy levels, the occupations per unit energy of the i-th site (i.e. (i, i) diagonal element of the occupation matrix in the site basis) is following:

$$n_i = s_i^2 n_{ss} + a_i^2 n_{aa} + s_i a_i (n_{sa} + n_{as}). \tag{20}$$

Here n_{ss}, n_{sa}, n_{as}, and n_{aa} are elements of the occupation matrix in the basis of symmetric and anti-symmetric states. If the sites i and j are mapped into each other by the mirror reflection σ_{LR} (i.e. $j = \sigma_{LR}(i)$), then corresponding components of the symmetric and anti-symmetric states must be: $s_i = s_j$ and $a_i = -a_j$. Therefore, the difference between occupations of this sites is

$$n_i - n_{\sigma_{LR}(i)} = 2s_i a_i (n_{sa} + n_{as}) \propto n_{sa} + n_{as}. \tag{21}$$

This difference appears to be proportional to the sum of non-diagonal elements of the occupation matrix in the symmetric/anti-symmetric states basis. Utilizing Eq. (19) we can calculate this sum for our system:

$$n_i - n_{\sigma_{LR}(i)} \propto n_{sa} + n_{as} = \frac{\Gamma\gamma_s\gamma_s(f_L - f_R)}{\pi[4\Gamma^2\gamma_a^4 + (\omega - \varepsilon - k_a\delta)^2][4\Gamma^2\gamma_s^4 + (\omega - \varepsilon - k_s\delta)^2]} \times |Q|, \tag{22}$$

where $|Q|$ is given by Eq. (18). Thus, it is obvious, that at perfect transmission resonances (real zeroes of Q) electron occupation is distributed symmetrically (with respect to σ_{LR} operation). Whereas, for energies, which correspond to complex roots of Q and transmission lower than 1, there is always asymmetric distribution of electrons. Therefore, $\mathcal{PT}$-symmetry breaking at the EP (coalescence of two perfect resonances into one non-perfect) manifests itself by a symmetry breaking of electron distribution, that was shown for linear systems in ref.[30].

Quantum interference inverter transfer characteristic. For a given general structure of the inverter one can calculate all terminal currents if certain voltages are applied. To do so, the transmission coefficients between the leads T_{1out}, T_{2out} and T_{12} should be determined first. Reference voltages V_{ref1} and V_{ref2} (assume $V_{ref1} < V_{ref2}$) are given by some external ideal voltage sources, i.e. we treat them as constants. As the input lead is

isolated from the system, the voltage V_{in} influences only transmission coefficients. For high-resistance loads the output voltage V_{out} is derived from the condition $I_{out}=0$, where I_{out} is the total current through the output lead, which is composed of the currents from the first and the second reference voltage leads (with appropriate sign).

Let us consider an inverter composed of two identical quantum switches ($\mathcal{PT}$-symmetric interference transistors). Assuming that resonance width is sufficiently small, we can approximate condition $I_{out}=0$ as follows:

$$\begin{aligned}&\left[f(\varepsilon_1 - eV_{out}) - f(\varepsilon_1 - eV_{ref1})\right] \times \frac{(\gamma_s^2+\gamma_a^2)[\delta_1^2(k_a-k_s)^2 + 4\Gamma^2(\gamma_a^2-\gamma_s^2)^2]}{\delta_1^2(k_a-k_s)^2 + 4\Gamma^2(\gamma_s^2+\gamma_a^2)^2}\\ =&\left[f(\varepsilon_2 - eV_{ref2}) - f(\varepsilon_2 - eV_{out})\right] \times \frac{(\gamma_s^2+\gamma_a^2)[\delta_2^2(k_a-k_s)^2 + 4\Gamma^2(\gamma_a^2-\gamma_s^2)^2]}{\delta_2^2(k_a-k_s)^2 + 4\Gamma^2(\gamma_s^2+\gamma_a^2)^2}.\end{aligned} \tag{23}$$

Here subscripts 1 and 2 correspond to the first and to the second quantum switches. Energies $\varepsilon_{1,2}$ are the energies of degenerate states in the first and in the second system respectively. Assume that they are adjusted to $\varepsilon_{1,2}=eV_{ref1,2}$, i.e. to the biased Fermi level of each reference lead. The applied input voltage influences parameters $\delta_{1,2}$ of the switches. The following model dependence of $\delta_{1,2}$ on the input voltage V_{in} provides a symmetrical transition from the "on"-mode to the "off"-mode of each quantum switch as V_{in} varies in the interval $[V_{ref1}, V_{ref2}]$:

$$\delta_{1,2} = \alpha(eV_{in} - \varepsilon_{1,2}), \tag{24}$$

where $0<\alpha<1$ is an electrostatic lever arm of the input lead (common gate). One can substitute Eq. (24) into Eq. (23) and derive the implicit dependence $V_{out}=V_{out}(V_{in})$, which is then used to get an expression for the gain (12).

References

1. Gimzewski, J. K. & Joachim, C. Nanoscale science of single molecules using local probes. *Sci.* **283**, 1683–1688, https://doi.org/10.1126/science.283.5408.1683, http://science.sciencemag.org/content/283/5408/1683.full.pdf (1999).
2. Aradhya, S. V. & Venkataraman, L. Single-molecule junctions beyond electronic transport. *Nat. Nanotechnol.* **8**, 399 https://doi.org/10.1038/nnano.2013.91. (2013).
3. Cuevas, J. C. & Scheer, E. *Molecular electronics: an introduction to theory and experiment* (World Scientific, 2010).
4. Aviram, A. & Ratner, M. A. Molecular rectifiers. *Chem. Phys. Lett.* **29**, 277–283, http://www.sciencedirect.com/science/article/pii/0009261474850311, https://doi.org/10.1016/0009-2614(74)85031-1 (1974).
5. Geim, A. K. & Novoselov, K. S. The rise of graphene. *Nat. Mater.* **6**, 183, https://doi.org/10.1038/nmat1849 (2007).
6. Alcón, I., Viñes, F., Moreira, Id. P. R. & Bromley, S. T. Existence of multi-radical and closed-shell semiconducting states in post-graphene organic dirac materials. *Nat. Commun.* **8**, 1957, https://doi.org/10.1038/s41467-017-01977-4 (2017).
7. Joachim, C. & Ratner, M. A. Molecular electronics: Some views on transport junctions and beyond. *Proc. Natl. Acad. Sci.* **102**, 8801–8808, https://doi.org/10.1073/pnas.0500075102, http://www.pnas.org/content/102/25/8801.full.pdf (2005).
8. Schwierz, F. Graphene transistors. *Nat. Nanotechnol.* **5**, 487, https://doi.org/10.1038/nnano.2010.89 (2010).
9. Zhao, M. *et al.* Large-scale chemical assembly of atomically thin transistors and circuits. *Nat. Nanotechnol.* **11**, 954, https://doi.org/10.1038/nnano.2016.115 (2016).
10. Han, S.-J. *et al.* High-speed logic integrated circuits with solution-processed self-assembled carbon nanotubes. *Nat. Nanotechnol.* **12**, 861, https://doi.org/10.1038/nnano.2017.115 (2017).
11. Cao, Q., Tersoff, J., Farmer, D. B., Zhu, Y. & Han, S.-J. Carbon nanotube transistors scaled to a 40-nanometer footprint. *Sci.* **356**, 1369–1372, https://doi.org/10.1126/science.aan2476, http://science.sciencemag.org/content/356/6345/1369.full.pdf (2017).
12. Iannaccone, G., Bonaccorso, F., Colombo, L. & Fiori, G. Quantum engineering of transistors based on 2d materials heterostructures. *Nat. Nanotechnol.* **13**, 183–191, https://doi.org/10.1038/s41565-018-0082-6 (2018).
13. Zhang, Y. *et al.* Direct observation of a widely tunable bandgap in bilayer graphene. *Nat.* **459**, 820, https://doi.org/10.1038/nature08105 (2009).
14. Miroshnichenko, A. E., Flach, S. & Kivshar, Y. S. Fano resonances in nanoscale structures. *Rev. Mod. Phys.* **82**, 2257–2298, https://doi.org/10.1103/RevMod-Phys.82.2257 (2010).
15. Lambert, C. J. Basic concepts of quantum interference and electron transport in single-molecule electronics. *Chem. Soc. Rev.* **44**, 875–888, https://doi.org/10.1039/C4CS00203B (2015).
16. Markussen, T., Stadler, R. & Thygesen, K. S. The relation between structure and quantum interference in single molecule junctions. *Nano Lett.* **10**, 4260–4265, https://doi.org/10.1021/nl101688a (2010).
17. Pedersen, K. G. L. *et al.* Quantum interference in off-resonant transport through single molecules. *Phys. Rev. B* **90**, 125413, https://doi.org/10.1103/Phys-RevB.90.125413 (2014).
18. Tsuji, Y., Hoffmann, R., Movassagh, R. & Datta, S. Quantum interference in polyenes. *The J. Chem. Phys.* **141**, 224311, https://doi.org/10.1063/1.4903043 (2014).
19. Solomon, G. C. Interference effects in single-molecule transport. In *Handbook of Single-molecule Electronics*, 341–369 (CRC Press LLC, 2015).
20. Fracasso, D., Valkenier, H., Hummelen, J. C., Solomon, G. C. & Chiechi, R. C. Evidence for quantum interference in SAMs of arylethynylene thiolates in tunneling junctions with eutectic ga-in (egain) top-contacts. *J. Am. Chem. Soc.* **133**, 9556–9563, https://doi.org/10.1021/ja202471m (2011).
21. Guédon, C. M. *et al.* Observation of quantum interference in molecular charge transport. *Nat. Nanotechnol.* **7**, 305, https://doi.org/10.1038/nnano.2012.37 (2012).
22. Vazquez, H. *et al.* Probing the conductance superposition law in single-molecule circuits with parallel paths. *Nat. Nanotechnol.* **7**, 663, https://doi.org/10.1038/nnano.2012.147 (2012).
23. Aradhya, S. V. *et al.* Dissecting contact mechanics from quantum interference in single-molecule junctions of stilbene derivatives. *Nano Lett.* **12**, 1643–1647, https://doi.org/10.1021/nl2045815 (2012).
24. Stafford, C. A., Cardamone, D. M. & Mazumdar, S. The quantum interference effect transistor. *Nanotechnol.* **18**, 424014 http://stacks.iop.org/0957-4484/18/i=42/a=424014 (2007).
25. Li, Y., Mol, J. A., Benjamin, S. C. & Briggs, G. A. D. Interference-based molecular transistors. *Sci. Reports* **6**, 33686, https://doi.org/10.1038/srep33686 (2016).
26. Gorbatsevich, A. A. & Shubin, N. M. Quantum analogs of cmos gates. *Usp. Fiz. Nauk (accepted)*, https://ufn.ru/en/articles/accepted/38346/, https://doi.org/10.3367/UFNe.2017.12.038310.
27. Jin, L. & Song, Z. Physics counterpart of the PT non-hermitian tight-binding chain. *Phys. Rev. A* **81**, 032109, https://doi.org/10.1103/PhysRevA.81.032109 (2010).

28. Gorbatsevich, A. A. & Shubin, N. M. Unified theory of resonances and bound states in the continuum in hermitian tightbinding models. *Phys. Rev. B* **96**, 205441, https://doi.org/10.1103/PhysRevB.96.205441 (2017).
29. Gorbatsevich, A., Zhuravlev, M. & Kapaev, V. Collapse of resonances in semiconductor heterostructures as a transition with symmetry breaking in an open quantum system. *J. Exp. Theor. Phys.* **107**, 288–301, https://doi.org/10.1134/S106377610808013X (2008).
30. Gorbatsevich, A. & Shubin, N. Coalescence of resonances in dissipationless resonant tunneling structures and –symmetry breaking. *Annals Phys*. **376**, 353–371, www.sciencedirect.com/science/article/pii/S0003491616302913 https://doi.org/10.1016/j.aop.2016.12.019 (2017).
31. Abe, M. Diradicals. *Chem. Rev.* **113**, 7011–7088, https://doi.org/10.1021/cr400056a (2013).
32. Tsuji, Y., Hoffmann, R., Strange, M. & Solomon, G. C. Close relation between quantum interference in molecular conductance and diradical existence. Proc. *Natl. Acad. Sci*. **113**, E413–E419, https://doi.org/10.1073/pnas.1518206113, http://www.pnas.org/content/113/4/E413.full.pdf. (2016).
33. Nozaki, D., Lücke, A. & Schmidt, W. G. Molecular orbital rule for quantum interference in weakly coupled dimers:Low-energy giant conductivity switching induced by orbital level crossing. *The J. Phys. Chem. Lett.* **8**, 727–732, https://doi.org/10.1021/acs.jpclett.6b02989 (2017).
34. Datta, S. Electronic Transport in Mesoscopic Systems. *Cambridge Studies in Semiconductor Physics* (Cambridge University Press, 1997) https://books.google.fr/books?id=28BC-ofEhvUC.
35. Ryndyk, D., Guti´errez, R., Song, B. & Cuniberti, G. Green function techniques in the treatment of quantum transport at the molecular scale. In *Energy Transfer Dynamics in Biomaterial Systems*, 213–335 (Springer, Berlin, Heidelberg, 2009).
36. Bender, C. M. Making sense of non-hermitian hamiltonians. *Reports on Prog. Phys.* **70**, 947 http://stacks.iop.org/0034-4885/70/i=6/a=R03 (2007).
37. Shimizu, A. *et al.* Aromaticity and [small pi]-bond covalency: prominent intermolecular covalent bonding interaction of a kekule hydrocarbon with very significant singlet biradical character. *Chem. Commun.* **48**, 5629–5631, https://doi.org/10.1039/C2CC31955A (2012).
38. Borden, W. T. & Davidson, E. R. Effects of electron repulsion in conjugated hydrocarbon diradicals. *J. Am. Chem. Soc.* **99**, 4587–4594, https://doi.org/10.1021/ja00456a010 (1977).
39. Carl Lineberger, W. & Thatcher Borden, W. The synergy between qualitative theory, quantitative calculations, and direct experiments in understanding, calculating, and measuring the energy differences between the lowest singlet and triplet states of organic diradicals. *Phys. Chem. Chem. Phys.* **13**, 11792–11813, https://doi.org/10.1039/C0CP02786C (2011).
40. Heeger, A. J., Kivelson, S., Schrieffer, J. R. & Su, W. P. Solitons in conducting polymers. *Rev. Mod. Phys.* **60**, 781–850, https://doi.org/10.1103/RevMod-Phys.60.781 (1988).
41. Theis, T. N. & Solomon, P. M. In quest of the next switch: Prospects for greatly reduced power dissipation in a successor to the silicon field-effect transistor. *Proc. IEEE* **98**, 2005–2014, https://doi.org/10.1109/JPROC.2010.2066531 (2010).
42. Ionescu, A. M. & Riel, H. Tunnel field-effect transistors as energy-efficient electronic switches. *Nat.* **479**, 329, https://doi.org/10.1038/nature10679. (2011).
43. Graham, A. *et al*. How do carbon nanotubes fit into the semiconductor roadmap? *Appl. Phys. A* **80**, 1141–1151, https://doi.org/10.1007/s00339-004-3151-7 (2005).
44. Peng, L.-M., Zhang, Z. & Wang, S. Carbon nanotube electronics: recent advances. Mater. Today **17**, 433–442, http://www.sciencedirect.com/science/article/pii/S1369702114002582, https://doi.org/10.1016/j.mattod.2014.07.008 (2014).
45. High, A. A., Novitskaya, E. E., Butov, L. V., Hanson, M. & Gossard, A. C. Control of exciton fluxes in an excitonic integrated circuit. *Sci*. **321**, 229–231, https://doi.org/10.1126/science.1157845, http://science.sciencemag.org/content/321/5886/229.full.pdf (2008).
46. Pirrotta, A., Solomon, G. C., Franco, I. & Troisi, A. Excitonic coupling modulated by mechanical stimuli. *The J. Phys. Chem. Lett*. **8**, 4326–4332, https://doi.org/10.1021/acs.jpclett.7b01828 PMID: 28837767 (2017).
47. Li, N. *et al.* Colloquium: Phononics: Manipulating heat flow with electronic analogs and beyond. *Rev. Mod. Phys.* **84**, 1045–1066, https://doi.org/10.1103/RevMod-Phys.84.1045 (2012).
48. Blanter, Y. & Buttiker, M. Shot noise in mesoscopic conductors. *Phys. Reports* **336**, 1–166, http://www.sciencedirect.com/science/article/pii/S0370157399001234. https://doi.org/10.1016/S0370-1573(99)00123-4 (2000).
49. Imry, Y. & Landauer, R. Conductance viewed as transmission. *Rev. Mod. Phys.* **71**, S306–S312, https://doi.org/10.1103/RevModPhys.71.S306 (1999).
50. Fisher, D. S. & Lee, P. A. Relation between conductivity and transmission matrix. *Phys. Rev. B* **23**, 6851–6854, https://doi.org/10.1103/PhysRevB.23.6851 (1981).
51. Caroli, C., Combescot, R., Nozieres, P. & Saint-James, D. Direct calculation of the tunneling current. *J. Phys. C: Solid State Phys.* **4**, 916 http://stacks.iop.org/0022-3719/4/i=8/a=018 (1971).
52. Meir, Y. & Wingreen, N. S. Landauer formula for the current through an interacting electron region. *Phys. Rev. Lett.* **68**, 2512–2515, https://doi.org/10.1103/PhysRevLett.68.2512 (1992).
53. Sokolov, V. & Zelevinsky, V. Collective dynamics of unstable quantum states. *Annals Phys*. **216**, 323–350 http://www.sciencedirect.com/science/article/pii/000349169290180T, https://doi.org/10.1016/0003-4916(92)90180-T (1992).

Acknowledgements

This work was supported in part by the Program of Fundamental Research of the Praesidium of the Russian Academy of Sciences.

Author Contributions

This work was planned, the results were discussed, and this report was completed by all three authors together. The calculations and analysis was mainly done by A.A.G. and N.M.S. All authors reviewed the manuscript.

Additional Information

Supplementary information accompanies this paper at https://doi.org/10.1038/s41598-018-34132-0.

Competing Interests: The authors declare no competing interests.

Publisher's note: Springer Nature remains neutral with regard to jurisdictional claims in published maps and institutional affiliations.